

Altimetry-Derived Gravity Predictions of Bathymetry by the Gravity-Geologic Method

JEONG WOO KIM,¹ RALPH R. B. VON FRESE,² BANG YONG LEE,³ DANIEL R. ROMAN,⁴ and SEONG-JAE DOH⁵

Abstract—The gravity-geologic method (GGM) was implemented for 2' by 2' bathymetric determinations in a 1.6° longitude-by-1.0° latitude region centered on the eastern end of the Shackleton Fracture Zone in the Drake Passage, Antarctica. The GGM used the Bouguer slab approximation to process satellite altimetry-derived marine free-air gravity anomalies and 6,548 local shipborne bathymetric sounding measurements from the Korea Ocean Research and Development Institute to update the surrounding off-track bathymetry. The limitations of the Bouguer slab for modeling the gravity effects of variable density, rugged bathymetric relief at distances up to several kilometers, were mitigated by establishing ‘tuning’ densities that stabilized the GGM predictions. Tests using two-thirds of the shipborne bathymetric measurements to estimate the remaining third indicated that the tuning densities minimized root-mean-square deviations to about 29 m. The optimum GGM bathymetry model honoring all the ship observations correlated very well with widely available bathymetry models, despite local differences that ranged up to a few kilometers. The great analytical simplicity of GGM facilitates accurately and efficiently updating bathymetry as new gravity and bathymetric sounding data become available. Furthermore, the availability of marine free-air gravity anomaly data ensures that the GGM is more effective than simply extrapolating or interpolating ship bathymetry coverage into unmapped regions.

Key words: Bathymetry prediction, gravity-geologic method, altimetry-derived gravity anomaly, Drake Passage, Antarctica.

1. Introduction

Extracting accurate ocean floor topography, or bathymetry, is essential for understanding the

evolution of the Earth. Conventional bathymetry mapping by shipborne surveys provides very accurate, but spatially limited views of the sea floor topography. More global views of the Earth's bathymetry began to emerge, however, as satellite marine altimetry from the Seasat mission became available (BECKER, 2008; DIXON *et al.*, 1983). In general, satellite radar altimetry-derived gravity anomalies can be used to estimate bathymetry because they mostly reflect the 15–200 km undulations of the sea floor topography (SANDWELL and SMITH, 2001, 2002; SMITH AND SANDWELL, 1994, 1997). Satellite radar altimetry maps mean sea surface heights from which geoid undulations or deviations of the geoid from the reference ellipsoid can be estimated (e.g., KIM, 1996). From the derived geoid undulations, free-air gravity anomalies can be estimated in the context of the disturbing potential.

Specifically, Bruns' formula (HEISKANEN AND MORITZ, 1967) relates geoid undulations, N in cm, and the disturbing potential, T in Gal × cm, by:

$$N = T/\gamma, \quad (1)$$

where γ is normal gravity in Gal. The disturbing potential, T , is the gravitational potential of mass that deviates from the standard homogeneous, ellipsoidal Earth. The fundamental equation of geodesy (HEISKANEN AND MORITZ, 1967) also relates the radial r -derivative of the disturbing potential and the gravity anomaly, Δg in Gal, by:

$$\Delta g = (-\partial T/\partial r) - 2T/R, \quad (2)$$

where R is the radius of the Earth in cm.

The gravitational acceleration (i.e., free-air gravity anomaly) is normal to the equipotential surface (i.e., geoid or mean sea surface). Thus, by measuring the equipotential surface from radar altimetry, we can calculate the gravity anomaly as well as the

¹ Department of Geomatics Engineering, University of Calgary, Calgary, AB T2N1N4, Canada. E-mail: jw.kim@ucalgary.ca

² School of Earth Sciences, The Ohio State University, Columbus, OH 43210, USA.

³ Korea Polar Research Institute, Incheon 406-840, Korea.

⁴ National Geodetic Survey, NOAA, 1315 East-West Highway, Silver Spring, MD 20910, USA.

⁵ Department of Earth and Environmental Sciences, Korea University, Seoul 136-713, Korea.

bathymetry where anomaly variations are caused purely by undulations of the ocean floor (FOWLER, 2005). However, gravity anomalies include the integrated effects of all crustal density variations, not just those of the topographic undulations. Thus, the need to separate gravity anomalies into their topographic components is a common consideration of gravimetric bathymetry studies (e.g., JUNG AND VOGT, 1992; GOODWILLIE AND WATTS, 1993; SMITH AND SANDWELL, 1994).

In this study, we investigated the utility of using the gravity effects of ship-measured bathymetry for estimating effective topographic components in the off-track altimetry-derived free-air gravity anomalies. This approach is an adaptation of the gravity-geologic method (GGM) that was applied effectively for mapping bedrock elevations beneath glacial drift deposits (IBRAHIM AND HINZE, 1972; ANDERSON, 1991; NAGARAJAN, 1994; ADAMS AND HINZE, 1995; KIM *et al.*, 2002). Here, we apply the GGM to extract improved bathymetry estimates in the Drake Passage, Antarctica, where shipborne measurements of ocean depth are sparse, but 2' by 2' satellite altimetry-derived gravity estimates are available.

Figure 1 shows generalized tectonic features of the Drake Passage, Antarctica, where the shaded rectangle delineates the study area (56.1° – 57.7° W; 60.25° – 61.25° S). The Drake Passage was formed by the separation of South America and the Antarctic Peninsula in the Oligocene (BARKER AND BURREL, 1997). The study area includes the structural triple junction composed of the Shackleton Fracture Zone (SFZ), the South Scotia Ridge (SSR), and the South Shetland Trench (SST). These tectonic features are well expressed in both the ocean bottom topography and local gravity anomalies.

For the Drake Passage, we used the altimetry-derived free-air gravity anomalies (FAGA) from SANDWELL AND SMITH (1997) that incorporated data from the Geosat and ERS1 altimetry missions. We also used local bathymetry estimates from shipborne echo sounding measurements obtained by the Korea Ocean Research and Development Institute (KORDI, <http://www.kordi.re.kr/>) during January 1993. We describe below the development of effective GGM bathymetric estimates from these data. We also test them against the KORDI data, as well as against the

bathymetry maintained in the global datasets by NOAA's National Geophysical Data Center (NGDC, <http://www.ngdc.noaa.gov/>) (NGDC, 2008a), SMITH and SANDWELL (1997), and Earth TOPOgraphical database 1 (ETOPO1, <http://www.ngdc.noaa.gov/mgg/global/global.html>) (NGDC, 2008b). In general, the GGM is applicable to any scale of gravity coverage. Thus, where higher frequency gravity data are available, the GGM can resolve shorter wavelength bathymetry than found in the global data sets.

2. Gravity-Geologic Method

The gravity-geologic method (GGM) was originally developed for predicting the depth-to-bedrock under lower density glacial drift deposits (IBRAHIM AND HINZE, 1972). As shown in Fig. 2, the procedure involves computing a regional gravity field g_{REG} from the depth-to-bedrock and Bouguer gravity anomaly (BGA) observations available at j -control points. At the other i -sites where depth-to-bedrock data are lacking, we subtract the regional anomaly field estimates from the BGA observations to generate residuals for estimating the bedrock undulations.

Local bedrock topography variations generate the shorter wavelength gravity field, g_{RES} , whereas deeper mass variations contribute to the regional gravity field, g_{REG} . These two components comprise the observed BGA given by:

$$g_{\text{OBS}}(i) = g_{\text{RES}}(i) + g_{\text{REG}}(i). \quad (3)$$

At the control points, we assume that the residual bedrock gravity effect g_{RES} may be modeled by the simple Bouguer slab formula as:

$$g_{\text{RES}}(j) = 2\pi G(\Delta\rho)(E(j) - D), \quad (4)$$

where G is the universal gravitational constant [$6.772 \times 10^{-11} \text{ m}^3/(\text{kg} \times \text{sec}^2)$], $\Delta\rho$ is the density contrast in g/cm^3 , and both the measured bedrock elevation $E(j)$ at the j -th control point and the reference datum elevation D are in meters. Bedrock elevations, $E(j)$, at the control points are typically available from borehole, seismic or other measurements, and the datum elevation, D , is commonly referenced to the deepest control point in the study area.

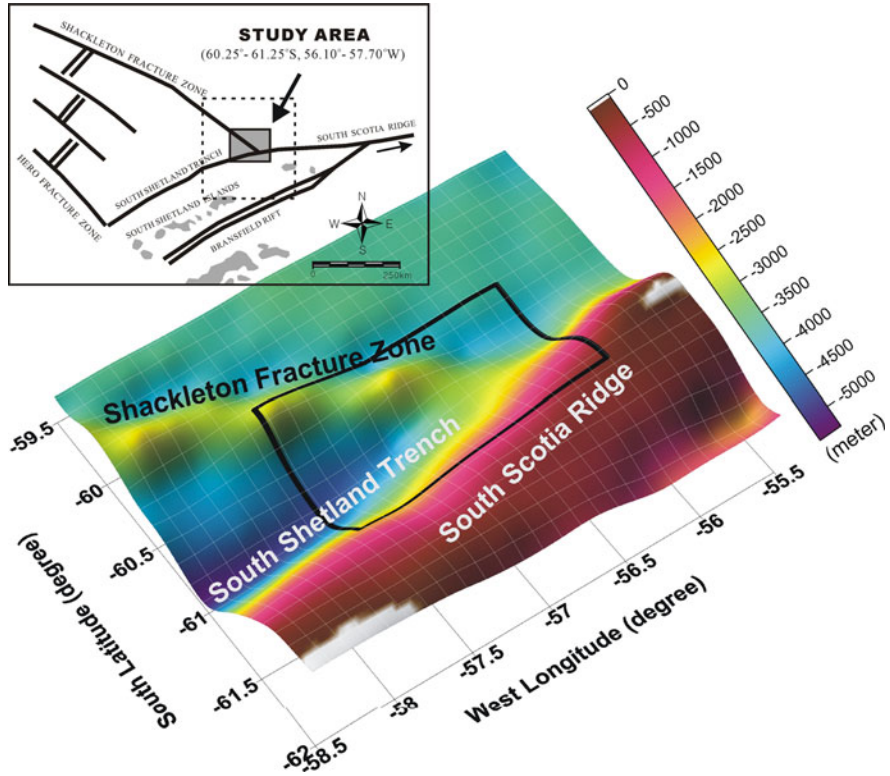


Figure 1

Shaded relief bathymetry (SMITH AND SANDWELL, 1997) with superposed tectonic features of the Drake Passage, Antarctica (modified from JEFFERS AND ANDERSON, 1990). The grey-shaded box outlined in black on the bathymetry delineates the study area

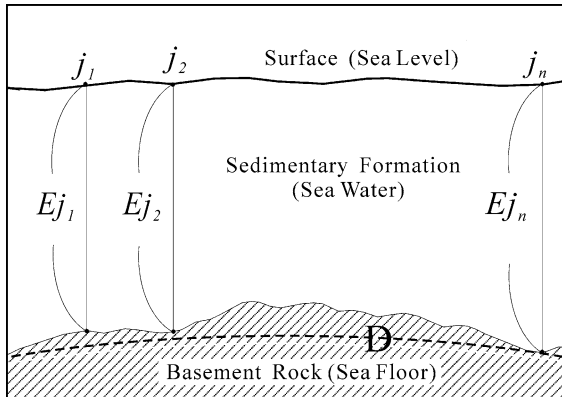


Figure 2
Geometry of gravity-geologic method (GGM)

At the control points, we rearrange Eq. 3 to estimate the regional gravity effects:

$$g_{\text{REG}}(j) = g_{\text{OBS}}(j) - g_{\text{RES}}(j). \quad (5)$$

The regional estimates determined at the sites, j , of measured bathymetry are gridded to generate the

regional gravity anomaly estimates, $g_{\text{REG}}(i)$, at the sites, i , of unmeasured bathymetry. The residual anomaly in turn is estimated by:

$$g_{\text{RES}}(i) = g_{\text{OBS}}(i) - g_{\text{REG}}(i). \quad (6)$$

Thus, by Eq. (4), bedrock surface variations can be obtained from:

$$E(i) = \frac{g_{\text{RES}}(i)}{2\pi G \Delta \rho} + D. \quad (7)$$

In general, the accuracy of GGM bedrock topography estimates is primarily influenced by the accuracy, number, and distribution of elevation control points and gravity observations, as well as by errors in the density contrast between bedrock and the overlying sediments (IBRAHIM AND HINZE, 1972; ADAMS AND HINZE, 1995; ANDERSON, 1991; NAGARAJAN, 1994; KIM *et al.*, 2002). Density errors are especially problematic where density variations within the bedrock and overlying drift deposits are

comparable to the density contrast assumed at the bedrock interface (HSIAO *et al.*, 2010)

For marine applications, the density contrast between seawater and the bathymetry generally is relatively much larger and more homogeneous than it is for terrestrial applications. However, the Bouguer slab approximation here is being implemented over distances up to a few kilometers in contrast to glacial bedrock applications that typically involve distances up to only a few hundred meters. Thus, the density contrast in the marine application is a far less physically realistic parameter than it is in mapping the much shallower bedrock relief. Indeed, for applications at altitude above the equivalent Bouguer slab, the tuning density may be considered as the slab density multiplied by the inverse ratio of the slab effect and its downward continuation to the top of the slab (STRYKOWSKI *et al.*, 2005). Thus, for bathymetry mapping, the tuning parameter allows the use of the equivalent source Bouguer slab to estimate regional gravity effects at the control points (Eq. 4) and bathymetry (Eq. 7). Furthermore, as shown in the next section, the control points can be readily analyzed for an appropriate tuning value of the density contrast to obtain effective bathymetric predictions.

An additional simplification of GGM marine applications is the direct use of the FAGA observations because they are located approximately at the geoid, and hence do not need to be corrected for elevation variations and related mass effects. In general, like in terrestrial implementations, the accuracy, number, and distribution of control points and gravity observations largely control the accuracy of GGM bathymetry estimates. However, the relative simplicity of the GGM considerably facilitates updating bathymetry estimates as the coverage in control points and gravity observations improves.

3. GGM Bathymetry Predictions in the Drake Passage

In this section, we obtain GGM estimates of the bathymetry for the area 56.1°W – 57.7°W and 60.25°S – 61.25°S in Fig. 1 of the Drake Passage, Antarctica. Figure 3 gives the $2'$ by $2'$ altimetry-derived FAGA from SANDWELL AND SMITH (1997). Black dots mark the distribution of the FAGA observations, g_{OBS} , and red dots mark the 15,580 shipborne measurements collected by NGDC

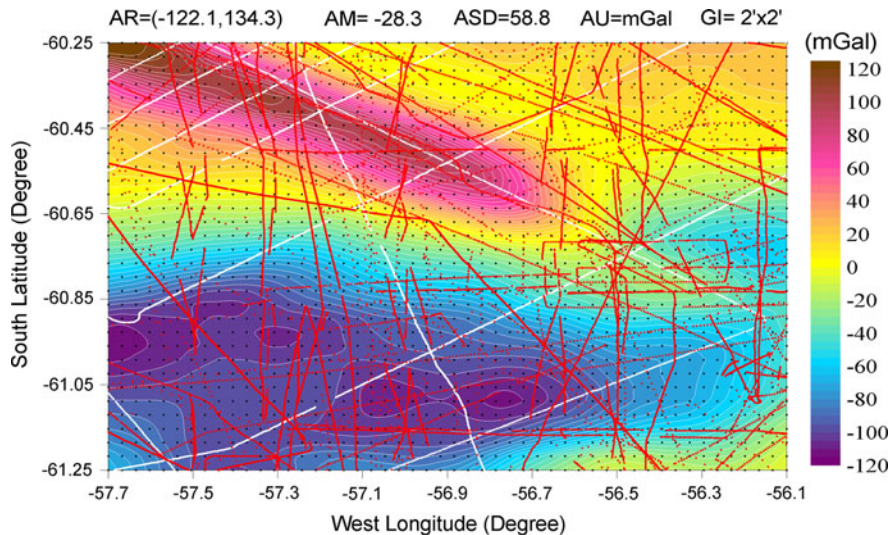


Figure 3

The $2'$ by $2'$ altimetry-derived free-air gravity anomalies by SANDWELL AND SMITH (1997) with superposed ship tracks used in this study. Red and white dots lies mark the 15,580 shipborne measurements collected by NGDC between 1962 and 2000, and the 6,548 bathymetric echo soundings collected by KORDI in 1993, respectively. Black dots delineate the gravity grid. Attributes listed for this and subsequent maps include the Amplitude Range (AR = (min, max)-values), Amplitude Mean (AM), Amplitude Standard Deviation (ASD), Amplitude Unit (AU), and Grid Interval (GI)

between 1962 and 2000, whereas white dots indicate the 6,548 bathymetric echo soundings collected by KORDI in 1993. The GGM bathymetric estimates were referenced to $D = -5,326$ m below sea level, which was the deepest elevation in the bathymetric measurements.

NAGARAJAN (1994) developed a procedure to identify effective tuning densities as part of an evaluation of the utility of GGM estimates for mapping the subglacial bedrock relief of Ohio (ODGS, 2003). The procedure can be extended to any application and involves determining and plotting the root-mean-squared (RMS) differences of GGM estimates as a function of increasing densities. Effective tuning densities are flagged where the differences level off and the GGM estimates are relatively stable or constant. The analysis used computer simulations to show that the tuning density produces minimal RMS errors of estimation. In general, the tuning density was found to have more analytical than physical significance because it essentially mitigates limitations in using a single-density Bouguer slab for analyzing multi-density terrain with rugged relief components that require gravity terrain corrections (NAGARAJAN, 1994).

Similar complications confront GGM efforts to map the multi-density, rugged bathymetry in the Drake Passage. An additional complexity of this application, however, is the great depth of the seafloor that averages over 3 km and limits the effectiveness of Bouguer slab approximations for modeling bathymetric gravity effects at sea level. Thus, following NAGARAJAN (1994), we investigated the stability of the GGM estimates to identify effective tuning densities. Specifically, we computed GGM estimates over a range of densities and obtained the RMS differences relative to the estimates for the geologically reasonable density contrast of 1.67 g/cm^3 between the 1.03 g/cm^3 -density of sea water and the rough 2.70 g/cm^3 -density of the bathymetry (JIN, 1995). The solid profile in Fig. 4 gives the differences that tend to level off or stabilize over tuning densities of about 9.0 g/cm^3 and greater.

These tuning densities also minimize RMS estimation errors as shown by the dashed profile in Fig. 4. This curve gives the RMS errors at every third control bathymetric point for GGM estimates that

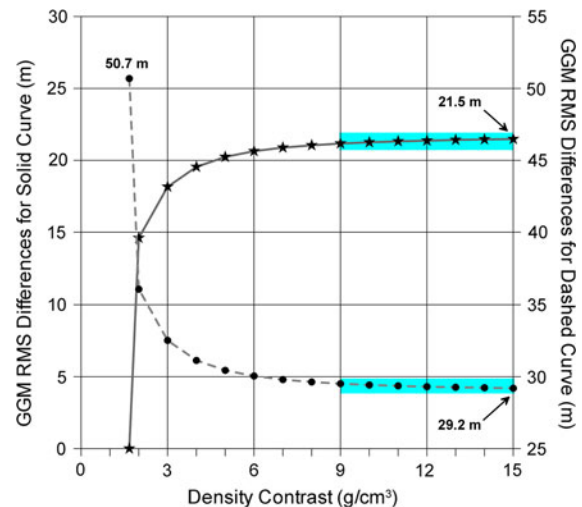


Figure 4
Trade-off diagram for selecting the tuning density contrast of 9.0 g/cm^3 in the study area. At values of 9.0 g/cm^3 and larger, the GGM estimates level off and stabilize (solid curve) and have minimal RMS differences with a third of the KORDI control data (dashed curve)

used only the other two-thirds of the shipborne measurements. It shows, for example, that using the geologically realistic density contrast of 1.67 g/cm^3 between sea water and bathymetry yields RMS errors of about 51 m, whereas tuning density contrasts of 9.0 g/cm^3 or greater reduce the errors to about 29 m. By virtue of the roughly 43% improvement in estimation accuracy suggested in the trade-off diagram of Fig. 4, we adopted the tuning density $\Delta\rho = 9.0 \text{ g/cm}^3$ for our GGM predictions in the Drake Passage.

Figure 5a gives the gridded regional gravity anomalies estimated from Eqs. 4 and 5 that were then subtracted from the observed FAGA in Fig. 3 to generate the residual FAGA in Fig. 5b. Applying Eq. 7 to these residual FAGA produced the $2'$ by $2'$ bathymetry predictions shown in Fig. 5c, which incorporate the KORDI's 6,548 shipborne bathymetric observations (shown in white lines in Fig. 3) for the Drake Passage study area.

4. Bathymetry Comparisons

Figures 6 and 7 facilitate comparing the GGM estimates in Fig. 5c against the other bathymetric

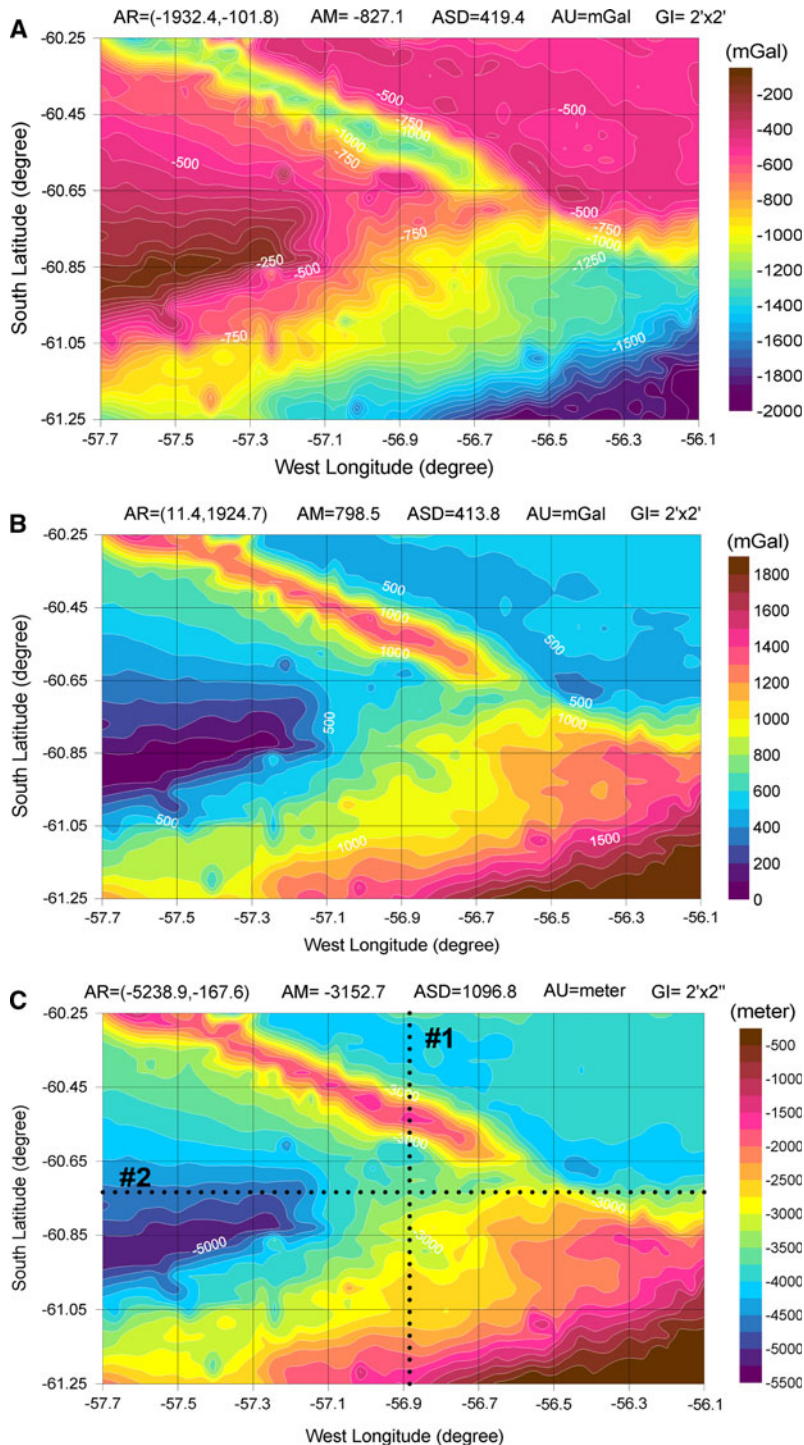


Figure 5

a Gives the regional gravity anomalies estimated from Bouguer slab approximations of the NGDC and KORDI shipborne measurements using the tuning density contrast of 9.0 g/cm^3 and gridded at $2'$ intervals by the minimum curvature algorithm (SMITH AND WESSEL, 1990). **b** Shows the residual gravity anomalies obtained by subtracting the regional anomalies from the altimetry-derived anomalies in Fig. 3. **c** Gives the GGM bathymetry estimates obtained from the residual anomalies in Map (b) by Eq. 7 with superposed profiles #1 and #2 that are compared in Figs. 8 and 9

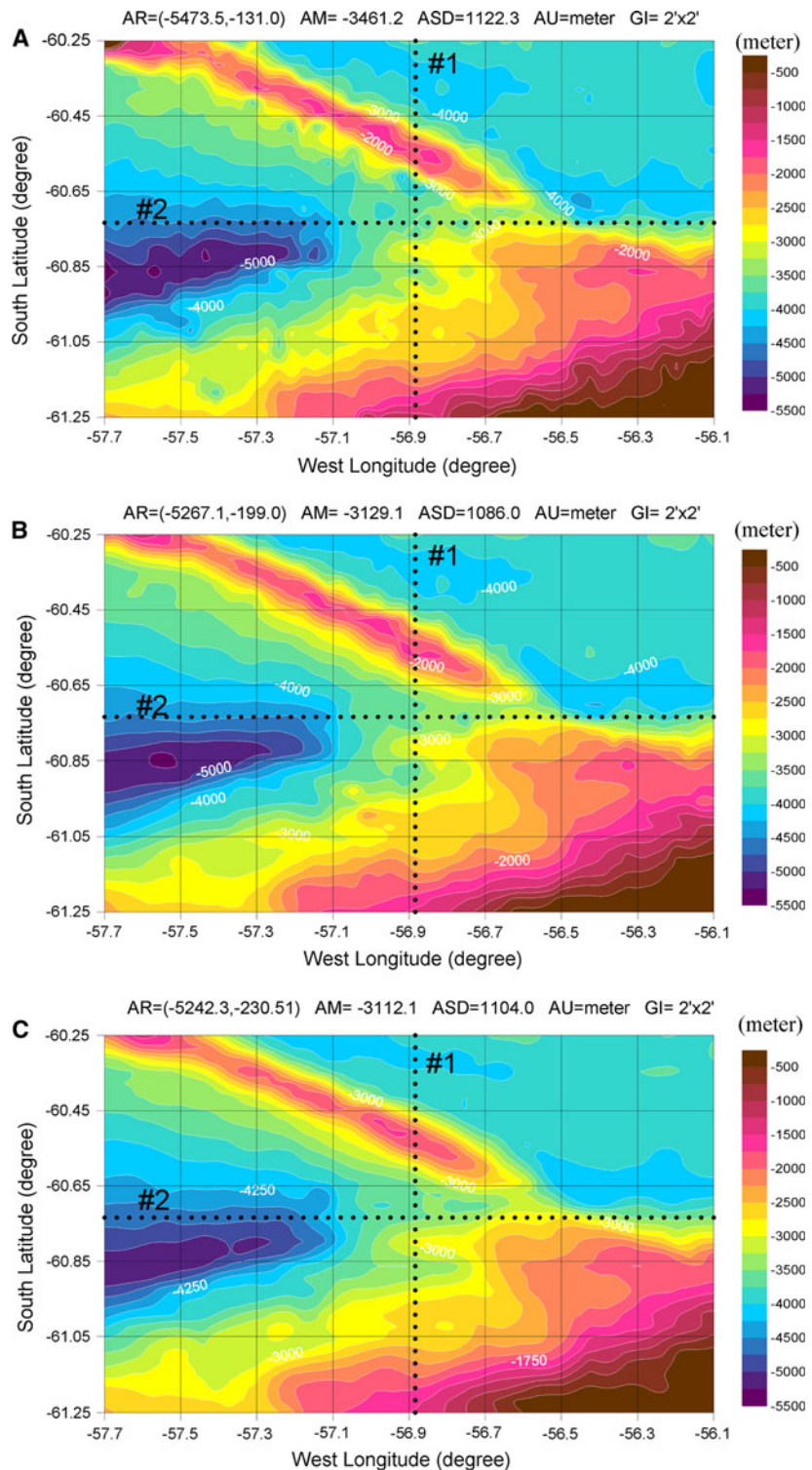


Figure 6

Bathymetry predictions from (a) combined NGDC and KORDI shipborne measurements gridded by minimum curvature, (b) SMITH AND SANDWELL (1997), and (c) ETOPO1. Bathymetry estimates from these data sets gridded onto profiles #1 and #2 by minimum curvature are contrasted in Figs. 8 and 9

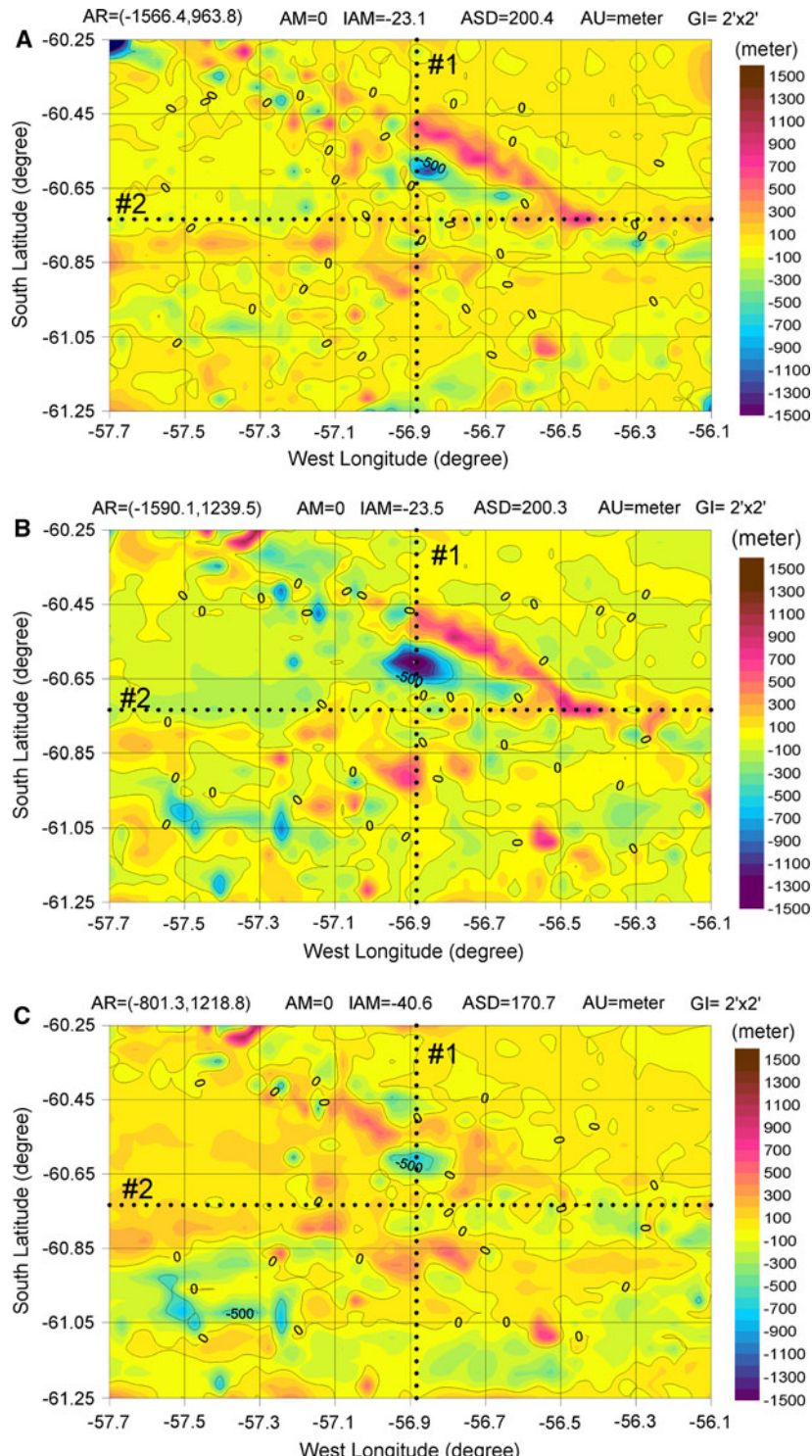


Figure 7

Comparisons of RMS bathymetry differences estimated from subtracting the respective maps in Fig. 6 from the GGM estimates in Fig. 5c. The initial amplitude mean (IAM) that was removed from each difference map is also listed. Bathymetry estimates along profiles #1 and #2 are contrasted in Figs. 8 and 9

predictions for the Drake Passage study area. In particular, Fig. 6 shows the estimates from (A) the combined GEODAS (NGDC, 2008a) and KORDI observations gridded by minimum curvature (SMITH AND WESSEL, 1990) (B) SMITH AND SANDWELL (1997), and (C) ETOPO1 (NGDC, 2008b), whereas Fig. 7 gives the respective differences obtained by subtracting the related maps in Fig. 6 from the GGM estimates in Fig. 5c. The difference contours and amplitude ranges (AR) in Fig. 7 reflect the removal of the initial amplitude mean (IAM) that is listed for each difference map.

In general, the bathymetric datasets in Figs. 5c and 6 all strongly express the raised topographic signature of the Shackleton Fracture Zone, but they differ substantially at the intersection of the fracture zone with the South Shetland Trench and South Scotia Ridge, as shown in Fig. 7. The consistency between Figs. 5c and 6a–c also is indicated by the strong correlation coefficients in the upper triangular matrix of Table 1. The GGM bathymetry model honoring all GEODAS and KORDI ship observations, for example, is correlated with the bathymetry models from the minimum curvature gridding of these data (shipborne), SMITH AND SANDWELL (1997) (S & S), and ETOPO1 at coefficients of 0.984, 0.983, and 0.988, respectively. However, the fact that the GGM predictions fully honor the shipborne observations does not guarantee the veracity of the GGM predictions where observations are lacking because

the gravity analysis does not produce unique results. Similarly, the other methods also yield non-unique predictions at unsurveyed locations that can be tested only by actual measurements.

Despite the general consistency of the various predictions, local point-by-point differences ranging up to several kilometers are evident in Fig. 7. The lower triangular matrix of Table 1 summarizes these differences in meters as RMS values (parentheses) and the associated difference ranges [brackets]. Figures 8 and 9 give additional insights on these local differences for the north–south transect #1 along -56.88°W and the east–west transect #2 along -60.73°S which intersect at the center of the study area as shown in Figs. 5c, 6 and 7. The profiles in Fig. 8 reveal relatively strong inconsistencies between the datasets across the Shackleton Fracture Zone, whereas significant mismatches between the predictions at the intersection of the fracture zone and South Shetland Trench and Scotia Ridge are illustrated in the profiles of Fig. 9.

In summary, the strong correlations between the gridded bathymetric models attest to the utility of the GGM for making effective bathymetry estimates. Despite these consistencies, non-unique bathymetric differences occur at unsurveyed locations for all the methods that ultimately can be tested only by actual measurements. However, these differences (e.g., Figs. 6, 7, 8, 9) clearly highlight critical regions where additional soundings can improve our understanding of the bathymetry of the Drake Passage

Table 1

Correlation matrix of the GGM, combined KORDI and NGDC shipborne (NGDC, 2008a), S & S (SMITH and SANDWELL, 1997), and ETOPO1 (NGDC, 2008b) bathymetry data

	GGM	Shipborne	S & S	ETOPO1
GGM	–	0.984	0.983	0.988
Shipborne	(13.3) [2530.2]	–	0.985	0.983
S & S	(25.8) [2829.6]	(12.5) [3079.1]	–	0.988
ETOPO1	(35.9) [2020.1]	(22.6) [2491.9]	(10.1) [1691.6]	–

The entries in the top triangular portion of the matrix give the relevant correlation coefficients. The bottom triangular matrix lists in meters the root-mean-squared (RMS) differences in (parentheses), and the [brackets] give the related range of the point-by-point differences

5. Conclusions and Recommendations

This study demonstrated the utility of the Gravity-Geologic Method (GGM) for bathymetric mapping in the Drake Passage, Antarctica. Although originally developed for mapping thickness variations of glacial drift, the GGM also has several advantages in marine applications. The universal availability of marine free-air gravity anomalies (FAGA) which include significant bathymetric effects, for example, ensures that the GGM can be more effective than simple gridding in extending ship bathymetric observations.

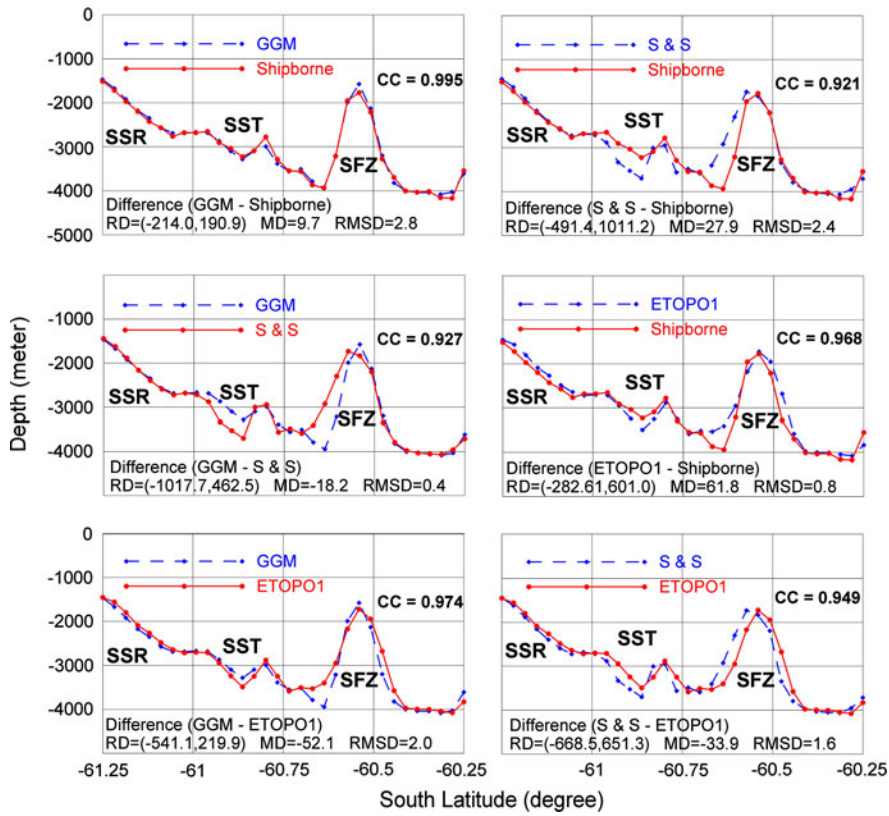


Figure 8
Bathymetry estimate comparisons for profile #1 along 56.88°W longitude as shown in Figs. 5c, 6, and 7. The *left column* compares the GGM estimates with the other model estimates, whereas the *right column* compares the other model estimates against each other. Each comparison in this and the next figure lists the range of the differences (RD), mean difference (MD), and RMS difference (RMSD). The Shackleton Fracture Zone (SFZ), the South Scotia Ridge (SSR), and the South Shetland Trench (SST) are also indicated

Francesco Ferrazzoli et al. / Pure and Applied Geophysics 172 (2015) 817–836

In addition, marine GGM applications involve the much stronger and more homogeneous density contrast between sea water and bathymetry. The depth to the marine density contrast also tends to be much deeper, and thus the marine Bouguer slab calculations are much less affected by the effects of subsurface density errors. However, the GGM can be effective with tuning densities that stabilize the RMS differences of the bathymetry predictions. Thus, the trade-off diagram in Fig. 4 established effective tuning densities of 9.0 g/cm³ and larger for the study area that also minimized bathymetric estimation errors when checked against a third of KORDI's control measurements.

The consistency of the GGM predictions with the bathymetry estimates from the other models also attests to the effectiveness of the GGM for

bathymetry mapping. Of course, the GGM predictions are not unique and thus the estimates must be used with care. However, the analytical simplicity of the GGM facilitates updating the bathymetric estimates as new details on the FAGA and bathymetric observations emerge.

An obvious focus for improving the GGM for bathymetry estimation is to replace the Bouguer slab formula with gravity models that more fully account for the geometric and density properties of the bathymetry (e.g., ASGHARZADEH et al., 2007). The trade-off, however, is that these efforts will supplant Eq. 7 with solutions of non-linear inverse problems that greatly enhance and complicate the analytical labor of implementing GGM for bathymetric mapping. However, the non-linear approach provides an option where greater bathymetric accuracy is desired.

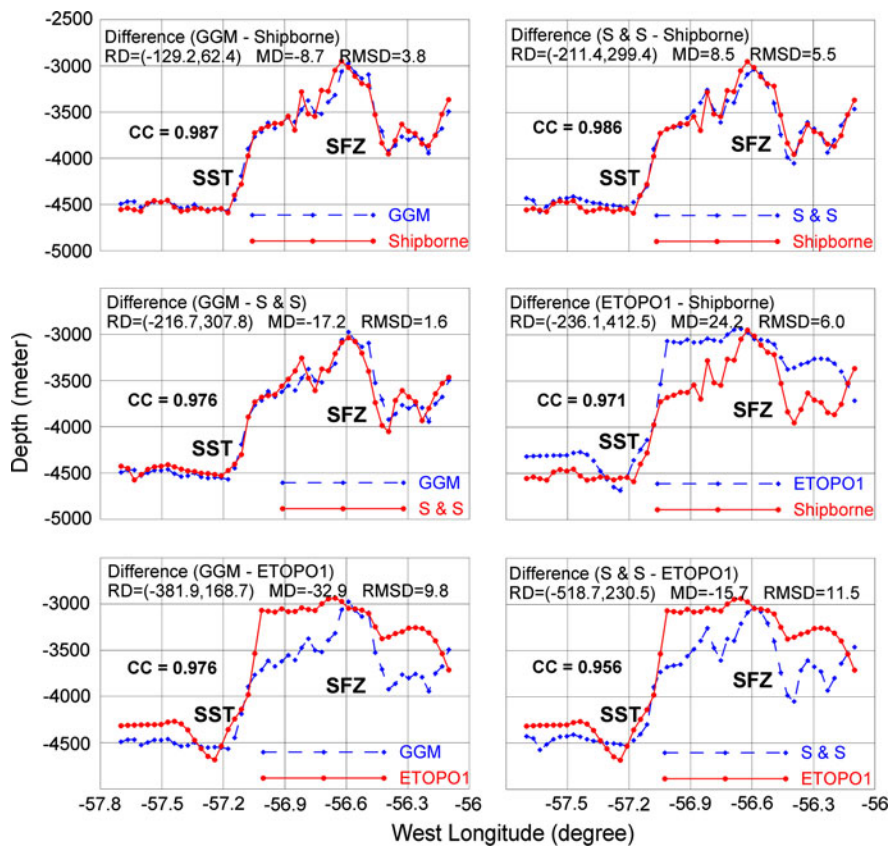


Figure 9

Bathymetry estimate comparisons for profile #2 along 60.73°S latitude as shown in Figs. 5c, 6, and 7. The left column compares the GGM estimates with the other model estimates, whereas the right column compares the other model estimates against each other

Acknowledgment

This study was supported by the COMPAC Project (#PE09030) of the Korea Polar Research Institute.

REFERENCES

- ADAMS, J.M. and HINZE, W.J., The gravity-geologic technique for mapping varied bedrock topography. In *Geotechnical and Environmental Geophysics* (ed. S.H. Ward) (Society of Exploration Geophysicists, Tulsa, OK, III, 99–106 1995).
- ANDERSON, G. (1991), *Use of the gravity-geologic method: Error propagation and case study*, unpublished M.S. thesis, Dept. of Geological Sciences The Ohio State University.
- ASGHARZADEH, M.F., VON FRESE, R.R.B., KIM, H.R., LEFTWICH, T.E., and KIM, J.W. (2007), *Spherical prism gravity effects by Gauss-Legendre quadrature integration*, Geophys J Int 169, 1–11.
- BARKER, P.F. and BURREL, J. (1997), *The opening of Drake Passage*, Mar Geol 25, 15–34.
- BECKER, J.J. (2008), *Improved Global Bathymetry, Global Sea Floor Roughness, and Deep Ocean Mixing*, Ph.D. Dissertation, University of California, San Diego.
- DIXON, T.H., NARAGHI, N., McNUTT, M.K., and SMITH, S.M. (1983), *Bathymetric prediction from Seasat altimeter data*, J Geophys Res 88, 1563–1571.
- FOWLER, C.M.R., *The Solid Earth* (2nd Ed.) (Cambridge University Press 2005).
- GOODWILLIE, A.M. and WATTS, A.B. (1993), *An altimetric and bathymetric study of elastic thickness in the central Pacific Ocean*, Earth Planet Sci Lett 118, 311–326.
- HEISKANEN, W.A. and MORITZ, H., *Physical Geodesy* (W.H. Freeman and Company San Francisco 364p, 1967).
- HSIAO, Y.S., KIM, K.B., KIM, J.W., LEE, B.Y., and HWANG, C. (2010), *Determination of Density Contrast for Bathymetry Estimation by the Gravity-Geologic Method*, J Marine Geodesy (in review).
- IBRAHIM, A. and HINZE, W.J. (1972), *Mapping buried bedrock topography with gravity*, Ground Water 10(3), 18–23.
- JEFFERS, J.D. and ANDERSON, A.B. (1990), Sequence stratigraphy of the Bransfield Basin, Antarctica, implication for tectonic history and hydrocarbon potential. In *Antarctic as an exploration*

- frontier—hydrocarbon potential, geology, and hazards* (ed. St. John, B.) Am Assoc Petroleum Geol Stud Geol 13, 13–29.
- JIN, Y.K. (1995), *Crustal structure of the South Shetland trench and the Shackleton fracture zone off the northern Antarctic Peninsula*, Ph.D. Dissertation, Seoul National University, 140p.
- JUNG, W.Y. and VOGT, P.R. (1992), *Predicting bathymetry from Geosat-ERM and shipborne profiles in the South Atlantic Ocean*, Tectonophysics 210, 235–253.
- KIM, J.W. (1996), *Spectral correlation of satellite and airborne geopotential field measurements for lithospheric analysis*, In Ph.D. Dissertation (unpubl.), Dept. of Geological Sciences, The Ohio State University, 171p.
- KIM, J.W., DOH, S.J., NAM, S.H., YOUN, S.W., and JIN, Y.K. (2002), *Gravity-Geologic Prediction of Bathymetry in the Drake Passage, Antarctica*, Korea Econ Environ Geol, 35(3), 273–284.
- NAGARAJAN, R. (1994), *Gravity-geologic investigation of buried bedrock topography in northwestern Ohio*, MS Thesis, Department of Geological Sciences, The Ohio State University, Columbus.
- NGDC (2008a), Marine trackline geophysics data CD-ROM set and Marine trackline search criteria selection U.S. Dept. of Commerce, NOAA, National Geophysical Data Center, Boulder, http://www.ngdc.noaa.gov/mgg/gdas/ims/trk_cri.html.
- NGDC (2008b), ETOPO1 Global Relief Model, U.S. Dept. of Commerce, NOAA, National Geophysical Data Center, Boulder, <http://www.ngdc.noaa.gov/mgg/das/dsignagrid.html>.
- ODGS (2003), Shaded bedrock topography of Ohio, Ohio Division of Geological Survey, Map BG-3, 1:500000.
- SANDWELL, D.T. and SMITH, W.H.F. (1997), *Marine gravity anomalies from Geosat and ERS-1 satellite altimetry*, J Geophys Res 102, B5, 10039–10054.
- SANDWELL, D.T. and SMITH, W.H.F., *Bathymetric estimation, in Satellite altimetry and earth sciences* (eds. Fu L.-L. and Cazenave A.) (Academic Press, San Diego, 69, pp 441–457 2001).
- SANDWELL, D.T. and SMITH, W.H.F. (2002), *Bathymetric estimation from altimetry*, In Proceedings of the International Association of Geodesy International Workshop on Satellite Altimetry, September 8–13, Wuhan, China.
- SMITH, W.H.F. and SANDWELL, D.T. (1994) *Bathymetric prediction from dense satellite altimetry and sparse shipboard bathymetry*, J Geophys Res 99, B11, 21,803–821,824.
- SMITH, W.H.F. and SANDWELL, D.T. (1997), *Global sea floor topography from satellite altimetry and ship depth soundings*, Science 277, 1957–1962.
- SMITH, W.H.F. and WESSEL, P. (1990), *Gridding with continuous curvature splines in tension*, Geophysics 55, 293–305.
- STRYKOWSKI, G., BOSCHETTI, F., and PAPP, G. (2005), *Estimation of the mass density contrasts and the 3D geometrical shape of the source bodies in the Yilgarn area, Eastern Goldfields, Western Australia*, J Geodyn 39, 444–460.

(Received June 12, 2009, revised May 3, 2010, accepted May 21, 2010, Published online June 29, 2010)